IOP PUBLISHING PHYSICS IN MEDICINE AND BIOLOGY

Phys. Med. Biol. **54** (2009) S1–S8 doi:10.1088/0031-9155/54/18/S01

A feasibility study of treatment verification using EPID cine images for hypofractionated lung radiotherapy*

Xiaoli Tang[1,2], **Tong Lin**[1,3] **and Steve Jiang**[1]

[1] Department of Radiation Oncology, University of California San Diego, La Jolla, CA 92093, USA
[2] Department of Radiation Oncology, University of North Carolina, Chapel Hill, NC 27514, USA
[3] Key Laboratory of Machine Perception (Ministry of Education), School of EECS, Peking University, Beijing 100871, People's Republic of China

E-mail: sbjiang@ucsd.edu

Received 20 March 2009, in final form 29 April 2009
Published 18 August 2009
Online at stacks.iop.org/PMB/54/S1

Abstract

We propose a novel approach for potential online treatment verification using cine EPID (electronic portal imaging device) images for hypofractionated lung radiotherapy based on a machine learning algorithm. Hypofractionated radiotherapy requires high precision. It is essential to effectively monitor the target to ensure that the tumor is within the beam aperture. We modeled the treatment verification problem as a two-class classification problem and applied an artificial neural network (ANN) to classify the cine EPID images acquired during the treatment into corresponding classes—with the tumor inside or outside of the beam aperture. Training samples were generated for the ANN using digitally reconstructed radiographs (DRRs) with artificially added shifts in the tumor location—to simulate cine EPID images with different tumor locations. Principal component analysis (PCA) was used to reduce the dimensionality of the training samples and cine EPID images acquired during the treatment. The proposed treatment verification algorithm was tested on five hypofractionated lung patients in a retrospective fashion. On average, our proposed algorithm achieved a 98.0% classification accuracy, a 97.6% recall rate and a 99.7% precision rate.

(Some figures in this article are in colour only in the electronic version)

1. Introduction

In the United States, lung cancer is the second most prevalent cancer and the leading cause of death from cancer, accounting for about 30% of all cancer mortality (Jemal *et al*

* This work was first presented at the Seventh International Conference on Machine Learning and Applications, San Diego, CA, USA, 11–13 December 2008.

2005). Hypofractionated lung radiotherapy is being increasingly employed as an alternate modality for the treatment of primary and secondary lung cancers. This therapy has the important advantages of allowing shortened treatment times while delivering higher effective radiobiological doses. However, normal tissues surrounding the tumors are also exposed to high-dose levels of radiation. Furthermore, cancerous tissue can occasionally move outside the irradiation field, e.g. when the patient has sudden irregular breathing or episodes of coughing. Under these circumstances, malignant tissue will be missed, and even more normal tissue than planned will be irradiated. A very large fractional dose (e.g. 10 Gy per fraction) is commonly applied in hypofractionated lung radiotherapy. This is in many ways an ablative therapy, both to the tumors and to the normal tissues surrounding them. Consequently, the precision requirement of hypofractionated lung radiotherapy is high. It is absolutely critical to effectively monitor the target to ensure maximal irradiation of the tumor with minimal irradiation of surrounding normal tissue.

The major uncertainty in treating lung cancer is the respiratory lung tumor motion, which can be clinically significant for some patients (e.g. of the order of 2–3 cm) (Jiang 2006). This uncertainty must be dealt with when delivering hypofractionated lung radiotherapy. Typically, margins are added to accommodate respiratory motion. However, even with margins, tumors, or portions of them, will occasionally move outside the irradiation field. Abrupt coughing, dramatically changing breathing patterns and sudden occurrences of pain, can all occur during treatment. Any one of these events can result in moving the tumor (or portions of it) outside the irradiation field. It is therefore critically important to constantly monitor the patients' treatment—and when the tumor is detected outside the irradiation field, the treatment must be temporarily stopped. The treatment should be resumed only when the tumor returns to the irradiation field or, in extreme cases, after patient re-setup.

EPID acquisition in the cine mode does not require any additional radiation dose, and yet the technique generates images that carry valuable information indicating the tumor position. Several methods for monitoring radiation therapy have been developed using cine EPID images, with or without implanted markers.

Berbeco *et al* developed a matching technique for respiratory-gated liver radiotherapy treatment verification with an EPID in the cine mode (Berbeco *et al* 2005, 2007). Implanted radio opaque fiducial markers inside or near the target were required for this technique. The markers were contoured on a planning CT set, enabling users to create digitally reconstructed radiographs (DRRs) for each treatment beam. During the treatment, a sequence of EPID images could be acquired without disrupting the treatment routine. Implanted markers were visualized in the images and their positions in the beam's eye view (BEV) were calculated off-line and compared to the reference position by matching the field apertures in corresponding EPID and DRR images. Tumor displacement was calculated for one patient with three implanted markers. The case study demonstrated the feasibility of the proposed method.

For lung cancer patients, implantation of fiducial markers is not widely acceptable due to the risk of pneumothorax (Laurent *et al* 2000, Arslan *et al* 2002, Geraghty *et al* 2003, Topal and Ediz 2003, Berbeco *et al* 2005). Arimura *et al* (2007) considered using cine EPID images for the measurement of displacement vectors of tumor positions in lung radiotherapy without implanted markers. A template-matching technique based on cross-correlation coefficients was proposed to calculate the similarity between a reference portal image and each cine EPID image. Five patients with non-small cell lung cancer and one patient with metastasis were included for a validation study. The proposed method worked well for four cases but not well for the other two.

To develop a more robust system, we propose an alternative approach for treatment verification of hypofractionated lung radiotherapy using cine EPID images without implanted

markers. An artificial neural network (ANN)-based technique will be developed to classify the cine EPID images into two classes: images with the tumor inside the radiation field and images with the tumor outside the radiation field.

This paper is organized as follows: section 2 will introduce methods and materials used in this work, including a brief introduction of ANN and a detailed description of how to apply ANN to our treatment verification problem. Section 3 presents experimental results. Section 4 will conclude this work and plan future work.

2. Methods and materials

The goal of online treatment verification is to monitor the tumor's position, to verify that it remains inside the radiation field (or beam aperture). If it is inside, the treatment can be continued. Otherwise, the treatment beam should be turned off. This observation provides us with a clue that the online treatment verification problem can in fact be modeled as a classification problem. EPID cine images corresponding to the tumor inside the aperture can be treated as one class, and EPID cine images corresponding to the tumor outside the aperture can be treated as another. In this work, we apply a machine learning algorithm, ANN, for treatment verification. We will test its feasibility off-line retrospectively for hypofractionated lung radiotherapy.

2.1. Artificial neural network

An artificial neural network is a mathematical model inspired by the way biological nervous systems process information. An ANN incorporates massively parallel systems with large numbers of interconnected simple processors, and it can solve many challenging computational problems. For a classification problem, an ANN will learn examples (training samples) of each class to extract corresponding patterns and detect unique trends. A trained ANN can therefore classify new samples into corresponding classes with high accuracy. More details on applying an ANN on cancer research can be found in work by Naquib and Sherbet (2001).

2.2. Training ANN

The first step of using any ANN is learning and training from samples. A trained neural network can be thought of as an 'expert' in the category of information it has been given to analyze. In our application of hypofractionated lung radiotherapy verification using cine EPID images, the ideal training samples would naturally be cine EPID images. There are, however, two problems. First, the ANN requires a large number of training samples to achieve reasonable results, and there are not enough cine EPID images generated during treatment to meet that standard. Second, to be able to verify the treatment using cine EPID images during treatment, the ANN training has to be completed before the treatment, when the cine EPID images are not yet available. For these reasons, cine EPID images cannot be used as training samples.

We generate training images from DRR to simulate cine EPID images with various artificially altered tumor locations. The DRRs were created in the BEV for each field. The field edges (MLC contours) were superimposed on these images. The first image in figure 1 illustrates an example of DRR of a treatment field. The solid red contour is the MLC contour. By shifting the MLC contour, the sub-image defined by the contour changes accordingly. If each sub-image is treated as a simulated cine EPID image, we can simulate cine EPID images with different tumor locations. Once again, consider the first image of figure 1: the blue and

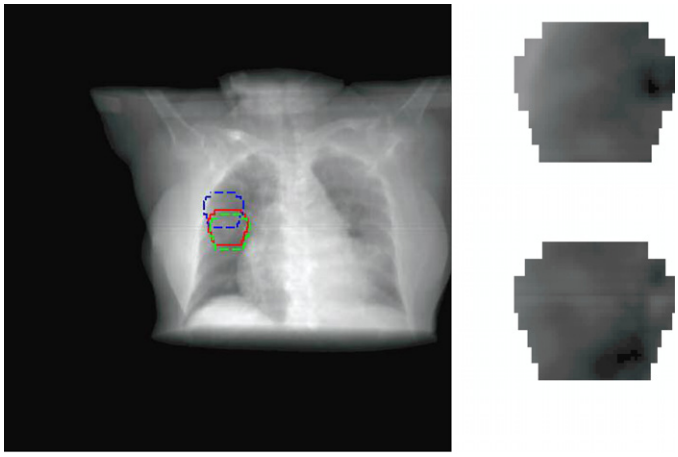

Figure 1. The image on the left shows DRR of a treatment field. The solid red contour is the MLC edge. The blue and green dashed contours define two examples of the training images for ANN. The sub-images inside the blue and green contours have been enlarged and displayed on upper right and lower right, respectively. All images are original without any image processing.

green dashed contours are two examples of the MLC contour at different locations. Tumor locations are different in the sub-images outlined by the corresponding contours. In this fashion, we can simulate cine EPID images with different tumor locations. The two images on the right side of figure 1 are the enlarged versions of the sub-images defined by the blue and green dashed contours in the first image, respectively. If we limit the MLC contour to move inside of an $m \times n$ pixel-sized window at the step size of 1 pixel, we can generate mn training images.

The clinical target volume (CTV) is defined by the physician on 4DCT and is projected onto each DRR. Based on the location of the CTV, we can calculate what percentage of the tumor is in the beam aperture of each training image. With a user-defined threshold $p\%$, we associate class 1 with the training image if more than $p\%$ of the tumor is in MLC, and class -1 otherwise.

From the total of mn training images, the ANN can learn what features indicate class 1 and what features indicate class -1. It can create its own organization or representation of the information it receives during the learning time. The trained network can therefore analyze the cine EPID images obtained during the treatment and classify them into the corresponding class 1 or -1. It is worth emphasizing again that we used DRR to simulate cine EPID images for training, and the classification was done on real cine EPID images.

2.3. Image processing

As we stated above, we used DRR instead of cine EPID images for neural network training. However, DRR and cine EPID images are different image modalities. Their pixel resolutions might be different, and their intensity values might be in different ranges. To enhance the ANN's performance, we applied image processing techniques to the DRR to make DRR and cine EPID images more closely resemble each other. First we either sub-sample or interpolate DRR to make its resolution the same as the cine EPID image, depending on the original resolution of DRR. Then, histogram equalization was applied on each DRR and cine EPID image to enhance image contrast. Finally, the intensity value of DRR was mapped to the

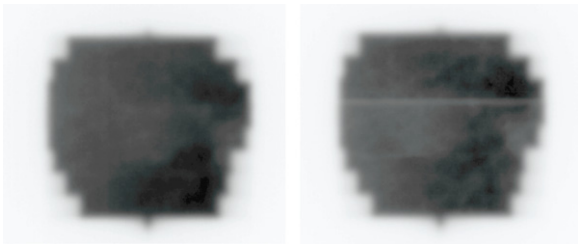

Figure 2. Examples of two original cine EPID images.

same range of cine EPID images. Based on our experience, pre-processing the images can significantly improve the ANN performance.

2.4. Principal component analysis (PCA)

A typical cine EPID image might have an approximate size of 100 × 100 pixels. This means that the dimensionality of a training sample would be 100 × 100 = 10 000. Significant computational time and resources would be needed to train the ANN with these high dimensional samples. This is simply not practical for online treatment verification. Consequently, PCA was applied to reduce the dimensionality of the training images. PCA is a classical statistical method. It involves a mathematical procedure that transforms original correlated variables into a small number of uncorrelated variables called principal components. The first principal component accounts for as much of the variability in the data as possible, and each succeeding component accounts for as much of the remaining variability as possible. In our application, we keep the first 15 principal components. Training 451 images with a reduced dimensionality of 15 using an un-optimized MATLAB program on a regular PC (Intel Xeon CPU with 2 GB RAM) resulted in a running time of less than 3 s, demonstrating the effectiveness of this refinement.

3. Experimental results

All hypofractionated lung radiotherapy patients included in this study were treated on a Varian Trilogy Linac (Varian Medical Systems, Palo Alto, CA, USA) equipped with an electronic portal imaging device. During the treatment, the EPID was set to acquire images in the cine mode at a frame rate of 0.625 Hz. Figure 2 shows two sample cine EPID images. The corresponding DRR is shown in figure 1.

Five patients each treated with four or five fractions were included in our feasibility study. Table 1 lists the related patient information. The average patient age is 70, and the average tumor volume is 10.04 cm^3. The total number of cine EPID images of each patient varies from 84 to 329 depending on the treatment time. The examples of the DRR and cine EPID images of patient 1 are displayed in figures 1 and 2. Figure 3 shows examples of the DRR and cine EPID images of patient 4. The red contour on the DRR defines the bean aperture. A window size of 40 × 10 pixels was used on each DRR to generate the training images. A radiation oncologist read the cine EPID images and manually classified them into classes 1 and −1, and this serves as our ground truth. A three-level feed-forward back propagation neural network was used. The network has a single hidden layer of ten neurons, and the network is trained for up to 50 epochs to an error goal of 0.01. The ANN was applied on the training images to build the neural network. We set $p = 95$ in this study—if more than 95% of the tumor projection is

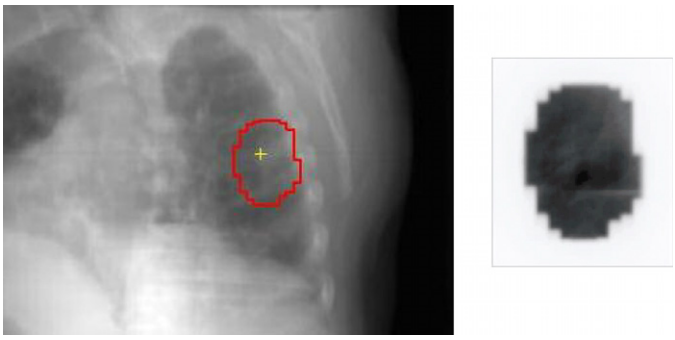

Figure 3. Original DRR and cine EPID image.

Table 1. Patient information.

Patient number	Age	Gender	Tumor location	Tumor volume (cm^3)
1	77	F	RUL	5.02
2	75	M	RUL	17.23
3	65	M	RUL	2.23
4	46	F	LLL	1.39
5	85	F	RLL	24.35
Average	70	–	–	10.04

inside the irradiation field, the corresponding training image is said to be in class 1. For each treatment field, one neural network needs to be built.

We would like to test if the proposed algorithm can successfully classify the cine EPID images corresponding to tumor outside the irradiation field obtained during the treatment. Those cine EPID images are category -1 images and also called true-negative images. However, since we were using real patient data retrospectively, we had very limited number of category -1 images. Therefore we simulated category -1 cine EPID images using the existing patient images.

Two patients whose tumor sizes were relatively small and treatment margins were large were selected for the simulation of category -1 images. For each treatment field, first we manually generated a sub-field inside the original field. As shown in figure 4(a), the yellow contour defines the sub-field which covers the tumor. Then we trained the ANN model based on this new simulated sub-field MLC contour. Since the sub-field is much smaller than the original field, there was enough room to simulate other sub-fields with the same size but different locations. Figures 4(b) and (c) are two examples of sub-fields with different locations, and they are examples of simulated category -1 cine EPID images. Figure 4(b) corresponds to the situation that approximately half of the tumor is outside of the beam aperture, and figure 4(c) corresponds to the situation that most of the tumor is not in the sub-field. The test cine EPID images include the simulated category -1 images as well as the category 1 images—images corresponding to the tumor inside the treatment sub-field as shown in figure 4(a). The trained ANN model will classify the test images into corresponding categories. The two cases with simulated category -1 cine EPID images are called cases 6 and 7.

We measure the accuracy, recall rate and precision of the classification results. They are defined as

$$\text{accuracy} = \frac{\text{true positive} + \text{true negative}}{\text{all}} \tag{1}$$

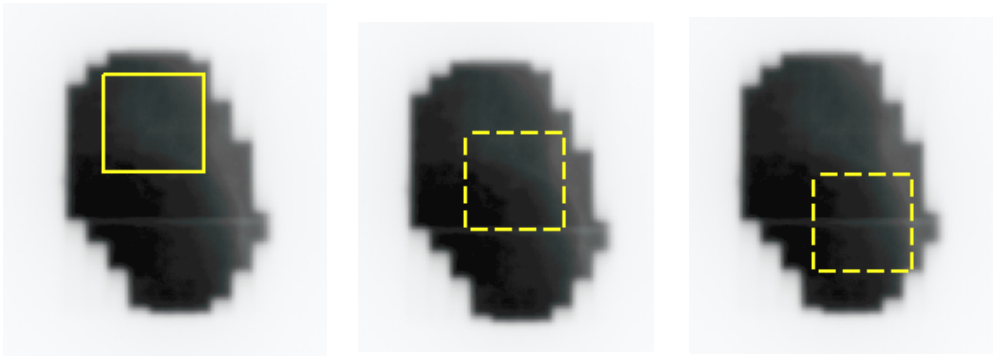

(a) (b) (c)

Figure 4. An example of generating a sub-field. (a) The generated sub-field is defined by the yellow contour; (b) and (c) are two examples of simulated true negative cine EPID images.

Table 2. Classification results in percentage.

Patient	Accuracy	Precision	Recall
1	94.12	100.00	94.12
2	99.87	98.86	98.89
3	97.00	100.00	97.00
4	98.86	99.87	98.89
5	98.91	100.00	98.91
Case 6	99.00	100.00	98.77
Case 7	98.13	99.08	96.43
Average	97.98	99.69	97.57

$$\text{precision} = \frac{\text{true positive}}{\text{true positive} + \text{false positive}} \tag{2}$$

$$\text{recall} = \frac{\text{true positive}}{\text{true positive} + \text{false negative}}. \tag{3}$$

Accuracy measures the degree of exactness or fidelity, precision measures the degree of reproducibility and recall measures the degree of completeness. False positive is defined as when the tumor projection was not in the beam aperture, but the classification result was of category 1. False negative is defined as when the tumor projection was in the beam aperture, but the classification result was of category -1.

Table 2 lists the classification results of all five patients and cases 6 and 7. Each number was averaged over all treatment fields. The average accuracy, precision and recall numbers over all the patients are also listed in the last row of the table.

For all cases, the results are good; the numbers are in the high nineties most of the time. Note that all the precisions are either 100% or close to 100%. This means that the reproducibility is high, and the proposed algorithm is stable. On average, the proposed algorithm achieved the accuracy of 97.98%, precision of 99.69% and recall of 97.57%.

4. Conclusion and future work

We have proposed a novel approach for online treatment verification for hypofractionated radiotherapy. The DRR was used to simulate cine EPID images for the ANN training. Image processing techniques were applied on the DRR to make the DRR and cine EPID images closely resemble each other. The PCA was also applied on training samples and cine EPID images acquired during the treatment to reduce their dimensionality in order to shorten the process time. We have tested our proposed algorithm on seven hypofractioned lung patient cases off-line in a retrospective fashion. The average accuracy and recall numbers are high, and the average reproducibility is close to 100%.

We intend to achieve even better results. More sophisticated image processing techniques will be applied to preprocess the DRR. We have already experienced a significant performance boost from pre-processing the images with the techniques described. Better image processing techniques should bring the classification accuracy rate even higher. All the ANN parameters were not optimized. We will investigate different combinations of parameters to find the set that yields the best performance. We used an empirical number 15 of principal components in this study. We plan to optimize the number of principal components in our future research. Now we use kV beam DRR. We are developing software to generate MV beam DRR with scattering effect which will better resemble cine EPID images obtained during the treatment. The number of cases tested is relatively small. We are collecting more patient data, hopefully with implanted fiducial markers, to further validate our proposed algorithm. Patients with variety of tumor volumes and locations will be selected. The performance of the algorithm will be analyzed based on tumor volume and location. Comparison will be made on different tumor volumes and locations.

References

Arimura H, Anai S, Yoshidome S, Nakamura K, Shioyama Y, Nomoto S, Honda H, Onizuka Y and Terashima H 2007 Computerized method for measurement of displacement vectors of target positions on EPID cine images in stereotactic radiotherapy *Med. Imaging* **6512** 65121U

Arslan S, Yilmaz A, Bayramqurler B, Uzman O, Nver E and Akkaya E 2002 CT-guided transthoracic fine needle aspiration of pulmonary lesions: accuracy and complications in 294 patients *Med. Sci. Monit.* **8** CR493–7

Berbeco R I, Hacker F, Ionascu D and Mamon H J 2007 Clinical feasibility of using an EPID in cine mode for image-guided verification of stereotactic body radiotherapy *Int. J. Radiat. Oncol. Biol. Phys.* **69** 258–66

Berbeco R I, Mostafavi H, Sharp G C and Jiang S B 2005 Towards fluoroscopic respiratory gating for lung tumours without radiopaque markers *Int. Phys. Pub.* **50** 4481–90

Geraghty P R, Kee S T, Mcfarlane G, Razavi M K, Sze D Y and Dake M D 2003 CT-guided transthoracic needle aspiration biopsy of pulmonary nodules: needle size and pneumothorax rate *Radiology* **229** 475–81

Jemal A, Murray T, Ward E, Samuels A, Tiwari R C, Ghafoor A, Feuer E J and Thun M J 2005 Cancer statistics *CA Cancer J. Clin.* **55** 10–30

Jiang S B 2006 Radiotherapy of mobile tumors *Semin. Radiat. Oncol.* **16** 239–48

Laurent F, Latrabe V, Vergier B, Montaudon M, Vernejoux J M and Dubrez J 2000 CT-guided transthoracic needle biopsy of pulmonary nodules smaller than 20 mm: results with an automated 20-gauge coaxial cutting needle *Clin. Radiol.* **55** 281–7

Naquib R N and Sherbet G V 2001 *Artificial Neural Networks in Cancer Diagnosis, Prognosis, and Patient Management* (Boca Raton, FL: CRC Press)

Topal U and Ediz B 2003 Transthoracic needle biopsy: factors effecting risk of pneumothorax *Eur. J. Radiol.* **48** 263–7